Continuously observing the spectrum of a dynamically decoupled spin-1 quantum gas

R. P. Anderson,[1] M. J. Kewming,[1] and L. D. Turner[1]

[1] *School of Physics & Astronomy, Monash University, Victoria 3800, Australia.*

(Dated: June 20, 2017)

Quantum states and spectra can be made sensitive to a particular measurand whilst simultaneously impervious to parasitic fluctuations of an environment. Here we use an atom-light interface with minimal backaction to probe the spectrum of a radiofrequency-dressed spin-1 quantum gas continuously and in-situ. The dressing amplitude sets the radiofrequency band in which oscillating magnetic fields manifest a linear measurand, and we probe the energy spectrum and coupling strengths during unitary evolution of the system. By varying a symmetry-breaking parameter of the Hamiltonian, we find a regime in which two of the dressed states are maximally insensitive (up to fourth-order) in magnetic field fluctuations that are slow compared to the dressed-state splittings. Moreover, we demonstrate the predictive power of our continuous probe to optimize the dynamical decoupling and tune the measurement band. This robust system shares the useful hallmarks of quantum metrology platforms; the states are thus termed ~~"synthetic clock"~~ 'synthetic clock' states in a complementary result by Dimitris et al. (arXiv:1706.xxxx) and are candidates for band-tunable magnetometry and emulation of quantum magnetism in solid-state systems.

From Hahn echoes to contemporary dynamical decoupling, abrupt, discrete rotations have been used to protect spin superpositions from inhomogeneities and parasitic fluctuations, prolonging quantum coherence and circumventing deleterious energy shifts [1–3]. A complementary strategy is to replace the pulse train with an uninterrupted coupling of 'bare' spin states, thus admitting new 'dressed' spin eigenstates, with a modified quantization direction, spectrum, and coupling, which too are protected from unwanted artifacts of their environment [4]. This *continuous* dynamical decoupling (CoDD) has proven useful across multiple platforms including nitrogen-vacancy centers [5–8] and superconducting qubits, and forms the basis for creating protected qubit [9] and decoherence-free [10] subspaces. Weak continuous measurement is a powerful instrument for appraising and refining dynamical decoupling in real time; to probe stochastic evolution, improve metrological bandwidth, or realize quantum feedback schemes [11].

Here we use dispersive optical readout of a 'bare' spin component $\hat{F}_x$ to measure the spectrum of a continuously decoupled spin-1 quantum gas using time-resolved Fourier spectroscopy. Fourier transform spectroscopy has been used to measure band structures of a spin-orbit coupled BEC [12] by composing multiple non-contiguous projective measurements. The rich time-frequency domain data in our experiment reveal not only multiple dressed-state splittings and their relative immunity to noise, but also dressed state coherences and coupling strengths. This potent ability to estimate the eigenspectrum of a multi-level dressed system reveals features absent in spin-1/2 or composite spin-1/2 qubit systems; principally, we identify a regime in which a subspace of the dressed system is maximally decoupled from noise $\propto \hat{F}_z$. This subspace is spanned by two of the dressed states, termed 'synthetic clock states' in a co-submission by Dimitris et al. (arXiv:1706.xxxx). The low-frequency magnetic stability and high-bandwidth detection of these states is immediately applicable to band-tunable (ac) magnetometry [5, 6, 13] and experiments preparing delicate spin-entangled many-body states [14]; whereas the unconventional cyclic coupling of all $2F+1$ dressed states could be applied to emulation of frustrated quantum spin chains [15].

Atomic Zeeman states $|m_z = -1, 0, 1\rangle$ in a magnetic field $B_z\mathbf{e}_z$ can be decoupled from fluctuations in B_z by applying a perpendicular radiofrequency (rf) field $B_{\rm rf}\mathbf{e}_x \cos\omega_{\rm rf}t$, oscillating at $\omega_{\rm rf}$, tuned near the Larmor frequency ~~$\omega_L = (E_{m_z=+1} - E_{m_z=-1})/2\hbar$~~ $\omega_L \equiv (E_{m_z=-1} - E_{m_z=+1})/2\hbar$. At low magnetic fields, the degeneracy of the composite spin-1/2 systems [16] renders the spin-1 behavior identical to CoDD in spin-1/2 systems. ~~In the dressed-state picture, the~~ The spin is quantized along ~~x;~~ $\mathbf{\Omega} = \Omega\,\mathbf{e}_x + \Delta\,\mathbf{e}_z$ in a frame rotating with the radiofrequency $\omega_{\rm rf}$~~the eigenstates~~; the eigenvalues of $\mathcal{H}_{\rm rwa} = \Delta\hat{F}_z + \Omega\hat{F}_x$ are ~~$|m_x = -1, 0, 1\rangle$, with energies~~ $m_x\hbar\sqrt{\Omega^2+\Delta^2}$, where $\Delta = \omega_{\rm rf} - \omega_L$ is the detuning and $\Omega = \gamma B_{\rm rf}/2$ is the Rabi frequency, and $|m_x = -1, 0, 1\rangle$ is the corresponding eigenstate at resonance $\Delta = 0$. Radiofrequency dressing induces an avoided crossing in the ~~dressed energy spectrum, at resonance $\Delta = 0$ reducing the leading-order sensitivity of the~~ spectrum; whereas the 'bare' state energies are linearly sensitive to magnetic field variations δB_z ($\omega_L \approx \gamma B_z$ where γ is the gyromagnetic ratio)~~to magnetic field variations δB_z from linear to quadratic.~~, the dressed energies are only quadratically sensitive near resonance.

The spin character and symmetries are otherwise unchanged: transverse magnetic fields oscillating near the splitting frequencies drive transitions between eigenstates. In the dressed system this means relatively low-frequency ('ac') fields oscillating near the Rabi frequency, such as $B_{y,\rm ac}\mathbf{e}_y \cos\Omega t$ and $B_{z,\rm ac}\mathbf{e}_z \cos\Omega t$, drive transi-

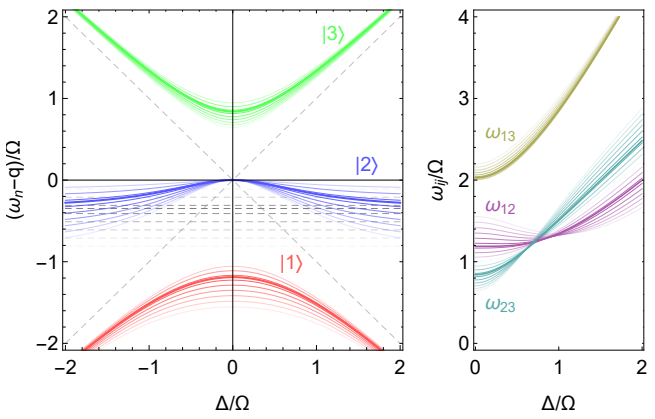

FIG. 1. Energy spectrum and splittings of a radiofrequency coupled spin-1 for various $q \in [0, \Omega]$. The transparency of each curve is proportional to the distance of q/Ω from $q_{R,\mathrm{magic}}$ in Eq. (1). (Left) Energies ω_n of dressed states $|n\rangle = |1\rangle$, (red) $|2\rangle$ (blue), and $|3\rangle$ (green) normalized to the rf-coupling strength (Rabi frequency) Ω as a function of detuning $\Delta = \omega_{\mathrm{rf}} - \omega_L$, Dashed lines indicate the energies of uncoupled states ($\Omega = 0$) in a frame rotating at ω_{rf}. (Right) Splittings ~~ω_{ij}~~ $\omega_{ij} = \omega_j - \omega_i$ of dressed states $|i\rangle$ and $|j\rangle$ as a function of detuning. When $q/\Omega = q_{R,\mathrm{magic}}$ (bold curves), energies ω_1 and ω_2 share the same curvature, and their difference ω_{12} (right, purple) is minimally sensitive to detuning and thus magnetic field variations.

tions $|m_x = -1\rangle \leftrightarrow |m_x = 0\rangle$ and $|m_x = 0\rangle \leftrightarrow |m_x = +1\rangle$. This is the basis for ac magnetometry [5] of relatively low-frequency fields; and for concatenated CoDD (CDD) which protects against fluctuations in Ω [7]. Insensitivity to wider bandwidth and larger amplitude δB_z can be achieved by increasing Ω, opening a broader gap in the dressed spectrum, but doing so changes the detection band of ~~the exquisitely sensitive quantum lock-in detection, recently demonstrated using NV centers~~ ac magnetometry using CDD [6] or pulsed dynamical decoupling [17]. Henceforth we presume Ω is fixed by the application. [Defer this?]

Any $\hat{F}_z^2$ interaction – ~~arising~~ from nonlinear Zeeman [18], microwave ac-Stark [19], or tensor light [20] shifts – raises the degeneracy of the $|m_z = -1\rangle \leftrightarrow |m_z = 0\rangle$ and $|m_z = 0\rangle \leftrightarrow |m_z = +1\rangle$ transitions~~, and breaks the symmetry of~~. Now $\mathcal{H}_{\mathrm{rwa}} = \Delta \hat{F}_z + \Omega \hat{F}_x + q\hat{F}_z^2/\hbar$, where the quadratic Zeeman shift $q \equiv (E_{m_z=+1} + E_{m_z=-1} - 2E_{m_z=0})_{\Omega=0}/2\hbar$. This yields dressed eigenstates $\{|1\rangle, |2\rangle, |3\rangle\}$ that are no longer SO(3) rotations of the bare Zeeman states $|m_z\rangle$, ~~but instead all have nematic order,~~ and an eigenspectrum $\omega_i(\Delta) = E_{|i\rangle}/\hbar$ shown in Fig. 1 (left).

Moreover, the couplings between these dressed states when $q \neq 0$ are markedly different: ~~the spin operators $\hat{F}_{x,y,z}$ represented in the dressed basis span more of SU(3) than for $q = 0$. The matrix element~~ $\langle 1|\hat{F}_{y,z}|2\rangle$ and $\langle 2|\hat{F}_{y,z}|3\rangle$ remain non-vanishing but $\langle 1|\hat{F}_x|3\rangle$ ~~is~~ becomes non-zero~~signifying direct coupling of dressed states $|1\rangle$ and $|3\rangle$, in contrast to the bare states where only adjacent states are coupled. Just as for bare states, we can characterize the splittings between dressed states near $\Delta = 0$~~. The transitions are thus cyclic ($|1\rangle \leftrightarrow |2\rangle \leftrightarrow |3\rangle \leftrightarrow |1\rangle$) and non-degenerate, characterized by a dressed Larmor frequency ~~$\omega_D = (\omega_3 - \omega_1)/2 = \sqrt{\Omega^2 + q_D^2}$~~ $\omega_D \equiv (\omega_3 - \omega_1)/2$, and dressed quadratic shift ~~$q_D = (\omega_3 + \omega_1 - 2\omega_2)/2 = -q/2$~~ $q_D \equiv (\omega_3 + \omega_1 - 2\omega_2)/2$, giving splittings $\omega_{23} = \omega_D - q_D$, $\omega_{12} = \omega_D + q_D$ and $\omega_{13} = 2\omega_D$. On resonance, $\omega_D = \sqrt{\Omega^2 + q_D^2}$ and $q_D = -q/2$.

A figure-of-merit for decoupling is the curvature of the transition frequency at resonance. In a dressed two-level system there is one convex and one concave eigenstate ~~and~~ whose splitting is simply convex. Figure 1 shows that in ~~our three-level~~ the spin-1 system with quadratic shift, two states are convex. ~~At a particular~~ This suggests that a regime may exist in which the curvature of their transition frequency vanishes [21]. Indeed we find an analytic value of the normalized quadratic shift $q_R = q/\Omega$ ~~the curvature is equal for $|1\rangle$~~ where the curvatures of ω_1 and ~~$|2\rangle$ and the curvature of ω_{12} vanishes. This 'magic' value is~~ω_2 are equal [22],

$$q_{R,\mathrm{magic}} = \sqrt{(3\sqrt{2} - 4)/2} \approx 0.348\,, \qquad (1)$$

resulting in the vanishing quadratic dependence of ~~their~~ the transition frequency $\omega_{12} = \omega_2 - \omega_1$ on Δ. The leading-order sensitivity of these states to field variations δB_z at $q_{R,\mathrm{magic}}$ is quartic [23], giving the subspace comprised of $|1\rangle, |2\rangle$ a higher-order decoupling than can be achieved with a two-level system; we join Dimitris et al. in terming these 'synthetic clock states'.

We ~~optimize of~~ explore this high-order decoupling in the laboratory with a continuous measurement of the dressed spectrum of a spin-1 non-degenerate quantum gas. Using a single realization of the quantum gas ~~, we adiabatically increase the detuning from resonance making many successive measurements, each of which simultaneously measures~~ we make many successive weak measurements, revealing all three splittings ω_{ij} ~~between the dressed states.~~ simultaneously. Our spinor quantum gas apparatus [24] and Faraday atom-light interface [25] are described elsewhere. We prepare an ultracold gas ($\sim 1\,\mu$K) of approximately 10^6 ^{87}Rb atoms in a crossed-beam optical dipole trap. A radiofrequency field of amplitude ~~$\Omega/(2\pi) \leq 100\,$kHz~~ $\Omega/2\pi \leq 100\,$kHz couples the three Zeeman states $|m_z = -1, 0, +1\rangle$ of the lowest hyperfine ground state. To perform a weak measurement of the evolving spin, we focus onto the atoms a linearly polarized far-off-resonant probe beam ~~($\lambda = 781\,$nm) onto the atoms. Any spin component transverse to the constant magnetic bias field rotates~~

~~the polarization~~ $\lambda = 781.15\,\mathrm{nm}$, red detuned $0.45\,\mathrm{THz}$) propagating along x. The spin component parallel to the wavevector of the probe rotates its polarization via the paramagnetic Faraday effect; shot-noise limited polarimetry ~~reveals~~ measures $\langle \hat{F}_x \rangle$ as an modulated tone near ω_L. Similar weak continuous ~~measurements using the paramagnetic Faraday effect have been used to observe~~ Faraday measurements have tracked spin-mixing dynamics of a polar spinor condensate [26] and ~~perform~~ enabled quantum state tomography ~~[20, 26].~~ [20, 26].

To probe the dressed state spectrum and coherences, we prepare a superposition of dressed states by suddenly turning on the Rabi coupling Ω~~at $t = 0$~~, projecting the polarized collective spin $|m_z = -1\rangle$ onto $|\psi(t = 0)\rangle = \sum_i c_i |i\rangle$. The total magnetic field in the laboratory frame ~~used to affect this control~~ is $\mathbf{B}(t \geq 0) = -B_{\mathrm{rf}} \cos(\omega_{\mathrm{rf}} t)\mathbf{e}_x + B_z(t)\mathbf{e}_z$, where $B_z(t)$ varies slowly compared to Ω. The resulting Faraday signal is ~~presented~~ analyzed in the time-frequency domain using the short-time Fourier transform (~~spectrogram~~STFT), revealing the rich frequency and amplitude modulation related to the dressed state energies, coherences, and coupling strengths. ~~For example, with~~

With no deliberate variation of the Rabi frequency or detuning, we observe the ~~spectrogram amplitude~~ STFT amplitude (spectrogram) shown in Fig. 2. Strong amplitude modulation of the Faraday signal is apparent ~~from the three upper and lower~~ as three pairs of sidebands, each ~~pair~~ equidistant from the carrier frequency ~~at $f_{\mathrm{rf}} = \omega_{\mathrm{rf}}/(2\pi)$~~ $f_{\mathrm{rf}} = \omega_{\mathrm{rf}}/2\pi$. Each pair of sidebands corresponds to a dressed state transition $|i\rangle \leftrightarrow |j\rangle$; with sideband frequencies $f_{\mathrm{rf}} \pm f_{ij}$ where ~~$f_{ij} = \omega_{ij}/(2\pi)$. In this way,~~ $f_{ij} = \omega_{ij}/2\pi$. Thus the spectrogram is a calibration-free, real-time measurement of the dressed state spectrum. Restricting attention to the upper sidebands, the two closest to the carrier are from adjacent state transitions ω_{12} and ω_{23} with similar amplitudes and ~~with frequency separations~~ at frequencies $\omega_D \pm q_D$ ~~from the carrierfor near-resonant coupling of the bare Zeeman states ($|\Delta| \ll \Omega$)~~above the carrier. The third, weaker sideband ~~near~~ $2\omega_D$ above the carrier signifies the cyclic $|1\rangle \leftrightarrow |3\rangle$ transition, appearing when $q \neq 0$. No attempt was made to shield the apparatus from ~~parasitic magnetic fields. Power line magnetic field noise~~ magnetic noise. The power line causes a temporally varying $\delta B_z = \delta B_{\mathrm{line}}(t)$ at the line frequency of $50\,\mathrm{Hz}$ and its odd harmonics, of ~~$\sim 1.4\,\mathrm{mG}$~~ $1.4\,\mathrm{mG}$ ($1\,\mathrm{kHz}$) peak-to-peak amplitude. ~~For these data $q_R = 0.402(3)$, and each~~ Each dressed transition is affected by the magnetic fluctuations differently: the sidebands corresponding to the ω_{13} and ω_{23} transitions exhibit asymmetric frequency modulation, whereas the optimally decoupled ω_{12} transition remains unperturbed within the frequency resolution of this spectrogram. ~~A plot of the normalised~~ The normalized power spectral density (~~PSD)~~ (Fig. 2, right) of the entire time-series yields maximum frequency resolution ~~(~~at the expense of all temporal resolution~~) and shows the~~. The ω_{12} transition is unskewed and has a near transform-limited width, four times narrower than the outwardly-skewed ~~peaks expected for transitions convex in Δ, e. g. the~~ ω_{23} ~~sidebands have a substantial third moments and a second moment (standard deviation) that is four times broader than the transform-limited peak of the ω_{12} transition.~~ and ω_{13} sidebands.

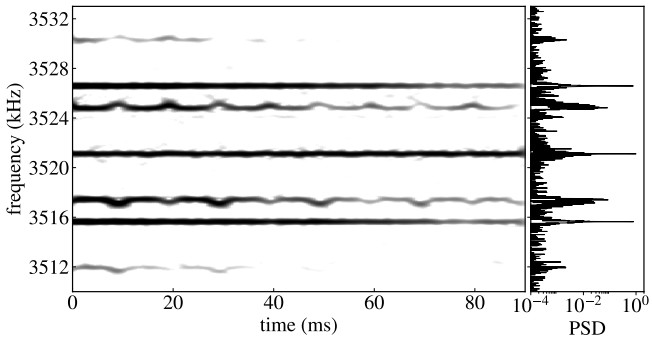

FIG. 2. Continuous measurement of the dressed energy spectrum for $q_R = 0.402(3)$, $f_{\mathrm{rf}} = 3.521\,\mathrm{MHz}$ and $B_0 = 5.013\,\mathrm{G}$ (left) and the power spectral density (PSD~~normalised to the highest peak~~, normalized) of the ~~100 ms~~ 90 ms long signal (right). (Inset) The dressed state energy diagram for resonant coupling ($|\Delta| \ll \Omega$); the mean and difference of transition frequencies ω_{12} and ω_{23} is the dressed Larmor frequency ω_D and quadratic shift q_D, respectively. The upper sidebands about the carrier at f_{rf} are associated with the ω_{13} (gold), ω_{23} (turquoise), and ω_{12} (lavender) transitions. ~~Magnetic field fluctuations $\delta B_z = \delta B_{\mathrm{line}}(t)$ of amplitude $1.4\,\mathrm{mG}$ induced by mains power are manifest as asymmetric frequency modulation of the ω_{13} and ω_{23} sidebands, while the ω_{12} transition remains relatively unaffected.~~ The corresponding spectral peaks have linewidths $102\,\mathrm{Hz}$, $97\,\mathrm{Hz}$, and $24\,\mathrm{Hz}$, respectively. The ω_{12} linewidth is near transform-limited, whereas the broadened peaks of the less decoupled ω_{23} transition exhibit a skew (third-moment) of $84\,\mathrm{Hz}$ (upper sideband) and $-100\,\mathrm{Hz}$ (lower sideband).

The amplitude of each sideband is proportional to the corresponding dressed-state coherence $\rho_{ij} = c_i^* c_j$, and ~~to the~~ the non-vanishing dressed state coupling~~strength induced by the spin projection operator~~(s) ~~$\hat{F}_{x,y,z}$ that give rise to the transition $|i\rangle \leftrightarrow |j\rangle$. $\langle i|\hat{F}_{x,y,z}|j\rangle$. An analytic expression for coupling~~ Analytic expressions for the sideband amplitudes near resonance (~~$\Delta \ll \Omega$) is~~ ($|\Delta| \ll \Omega$) are summarized in Table I. ~~These depend on the initial~~ If the projection onto the dressed basis ~~, which if knownamounts to continuous measurement of all coupling strengthsin the dressed basis, effecting Hamiltonian parameter estimation for the dressed-system couplings.~~ (and hence ρ_{ij}) is known, our measurement constitutes a single-shot estimation of the coupling strengths. Alternatively, if the ~~dressed state~~ couplings are separately characterized [27], this amounts to ~~real-time~~ continuous measurement of the dressed den-

TABLE I. Upper sidebands of the carrier (at $\omega_{\rm rf}$) of the Faraday rotation signal $\propto \langle \hat{F}_x \rangle$ of an arbitrary dressed state superposition driven on resonance ($\Delta = 0$). Frequency and phase are reported relative to the carrier, along with the transition that each sideband corresponds to. For the initial state $|\psi(t=0)\rangle = |m_z = -1\rangle$, the sideband frequencies and amplitudes can be concisely expressed in terms of the dressed Larmor frequency ω_D and quadratic shift q_D. For each upper sideband, there is a lower sideband of the same amplitude, relative frequency and opposite relative phase.

transition	frequency	$\omega_{ij} - \omega_{\rm rf}$ ($\Delta = 0$)	amplitude ($\Delta = 0$)	amplitude ($\Delta = 0$, $\lvert m_z = -1\rangle$)
(carrier)	$\omega_{\rm rf}$	0	$(\langle 3\lvert\hat{F}_x\rvert 3\rangle - \langle 1\lvert\hat{F}_x\rvert 1\rangle)(\rho_{33} - \rho_{11})$	$\hbar q_D \Omega / 2\omega_D^2$
$\lvert 1\rangle \leftrightarrow \lvert 2\rangle$	$\omega_{\rm rf} + \omega_{12}$	$\omega_D + q_D$	$-2i\langle 1\lvert\hat{F}_y\rvert 2\rangle \mathrm{Re}\,\rho_{12} = -2\langle 2\lvert\hat{F}_z\rvert 3\rangle \mathrm{Re}\,\rho_{12}$	$\hbar\Omega/4\omega_D$
$\lvert 2\rangle \leftrightarrow \lvert 3\rangle$	$\omega_{\rm rf} + \omega_{23}$	$\omega_D - q_D$	$2i\langle 2\lvert\hat{F}_y\rvert 3\rangle \mathrm{Re}\,\rho_{23} = 2\langle 1\lvert\hat{F}_z\rvert 2\rangle \mathrm{Re}\,\rho_{23}$	$\hbar\Omega/4\omega_D$
$\lvert 1\rangle \leftrightarrow \lvert 3\rangle$	$\omega_{\rm rf} + \omega_{13}$	$2\omega_D$	$2\langle 1\lvert\hat{F}_x\rvert 3\rangle \mathrm{Re}\,\rho_{13}$	$\hbar q_D \Omega / 4\omega_D^2$

sity matrix, effecting quantum state estimation of the dressed system. ~~Metrics~~

Different platforms use different metrics for the fidelity of dynamical decoupling~~vary amongst platforms~~, and in addition to linewidth narrowing include prolonged coherence. We ~~nominally~~ observe a three-fold increase in the lifetime of the spectral components corresponding to the ω_{12} and ω_{23} transitions as compared with the undressed system (Fig. 3a, $1/e$ decay time 23.8(2) ms). ~~The dressed-state~~ Dressed-state coherences are expected to ~~be greater~~last longer, but were limited here ~~to $\sim$ 100 ms by~~ by the $\sim$ 100 ms probe-induced photon scattering ~~; admitting a lower signal-to-noise ratio using~~ time. A less perturbative probe [25] ~~would permit longer coherences to be revealed. To appraise the success of~~ should reveal even longer dressed coherence times at the expense of signal-to-noise ratio.

To better expose the enhanced decoupling of the ~~dressed state transitions, and their dependence on the quadratic shift q_R, we varied the~~ synthetic clock states in the vicinity of $q_{R,\rm magic}$, we swept the the magnetic field over a wider range than was furnished by ~~our~~ the power line noise~~of , by sweeping the bias magnetic field along z over a range $B_{\rm rf}$ during the measurement interval. The control~~ . The longitudinal field $B_z(t) = B_0 + \alpha t + B_{\rm line}(t)$, where $\alpha = 128\,\mathrm{mG/s}$ is the linear sweep rate; the resulting detuning ~~variation is of order~~ sweeps across 2Ω (*cf.* the domain of Fig. 1) ~~. For each~~ during the single-shot measurement. We interleave each dressed state realization (or 'shot') of the experiment ~~, we calibrate~~ with a magnetometry shot calibrating $B_z(t)$~~using magnetometry of the bare Zeeman states~~: an rf $\pi/2$-pulse ~~(rather than continuous coupling)~~ initiates Larmor precession of the ~~collective spin in the x-y plane~~undressed collective spin, and the Faraday signal is composed of two tones at $\omega_\pm = \omega_L \pm q$, the ~~bare~~ Zeeman splittings (Fig. 3, top). For $q\,\tau_f \geq 2\pi$, where τ_f is the length of the spectrogram window, ~~the two tones are spectrally resolved and their mean and difference yields ω_+~~ are resolved yielding the instantaneous $\omega_L(t)$ and $q(t)$~~, respectively~~. We then use ~~ω_L~~ $\omega_L(t)$ to find $\delta B_z(t)$ (and $\Delta(t)$) by inverting the Breit-Rabi equation [18] [28].

We measured the dressed spectrum for resonant magnetic fields B_0 ranging from ~~3.549 to 5.568 G~~ 3.549 to 5.568 G (applied rf frequencies $f_{\rm rf}$ from ~~2.493~~ 2.493 to 3.911 MHz), with a ~~fixed~~ mean Rabi frequency of ~~$\Omega/(2\pi) = 4.505(3)$ kHz~~ $\Omega/2\pi = 4.505(3)$ kHz ($B_{\rm rf} = 12.83(1)$ mG). At each field B_0 we ensured the Rabi frequency was fixed by measuring the voltage drop across the coil at $f_{\rm rf}$ with an rf lock-in amplifier~~which — in concert with an impedance analyzer — could be used to ensure the rf current in the coil and thus Ω was constant.~~ . The Rabi frequency was ultimately measured using the atoms by analyzing ~~a subset of~~ the dressed energy spectrum ~~during the magnetic field sweep when $|\Delta|/(2\pi) \leq 100$ Hz.~~ near resonance ($|\Delta|/2\pi \leq 100$ Hz) where $\Omega = \sqrt{\omega_{12}\omega_{23}}$. The measured Rabi frequencies had a standard deviation ~~$\sigma(\Omega) = 9.4$ Hz~~$\sigma(\Omega)/2\pi = 9.4$ Hz, validating the above method.

~~The dressed spectrum for the swept control field with resonant field $B_0 = 5.013$ G and $q_R = 0.403(2)$ is shown in b.~~ Figure 3 shows the dressed spectrum measured as δB_z varies across a range $B_{\rm rf}$ during a single-shot. The instantaneous dressed state splittings for all three transitions were predicted with no free parameters, and are plotted atop the spectrogram data, showing excellent agreement with the measured sidebands. ~~Because~~ Line noise renders $\delta B_z(t)$ ~~is non-linear~~ neither linear nor monotonic. By tracking the instantaneous peaks in the calibration and ~~non-monotonic in time, we use the raw time series from the calibration ($\Omega = 0$) and CoDD shots to form parametric~~ dressed spectrograms we plot $(\delta B_z(t), f_{ij}(t))$ ~~data, by tracking the instantaneous peaks in each spectrogram~~parametrically, eliminating the line noise systematic. The sensitivity of the $|1\rangle \leftrightarrow |2\rangle$ and $|2\rangle \leftrightarrow |3\rangle$ transitions to magnetic field variations ~~are~~ is shown in Fig. 3c. The synthetic clock transition is most insensitive; ~~the measured predicted~~ f_{12} varies by 39 Hz (expt.), 26 Hz (theory) for $0 \leq \delta B_z \leq B_{\rm rf}/4 = 3.2$ mG (Fig. 3c, inset). ~~The corresponding normalized variation in~~ Normalizing the variation to the Rabi frequency makes possible a comparison of the decoupling across platforms

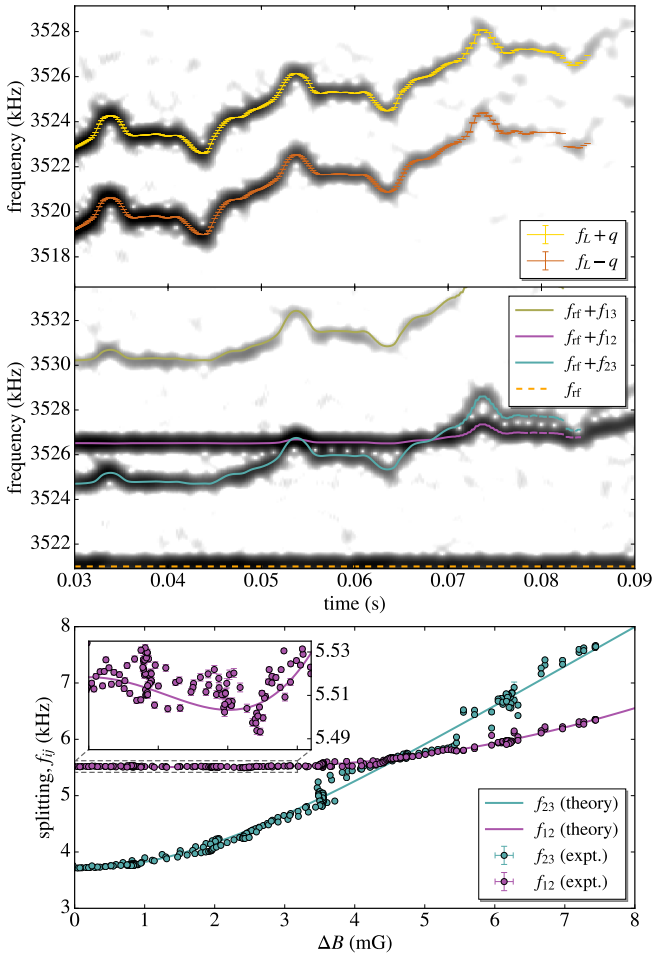

FIG. 3. Real-time CoDD observation for $q_R = 0.402(3)$. (a) and (b) are spectrograms of a continuous weak measurement of $\langle \hat{F}_x \rangle$. (a) Magnetometry of the bare Zeeman states ($\Omega = 0$) used to calibrate $B_z(t) = B_0 + \delta B_z(t)$ over the interrogation interval, in which the field [detuning] varies over a range $\sim B_{\rm rf}$ [2Ω]. We numerically track the bare Zeeman splittings (gold/orange) to determine the instantaneous Larmor frequency $f_L(t)$ and quadratic shift $q(t)$. (b) The field is swept over the same range but the rf dressing is applied ($\Omega > 0$). Three sidebands above (shown) and below the carrier at $f_{\rm rf} = 3.521\,$MHz (dashed, orange) reveal the dressed state splittings $f_{ij} = \omega_{ij}/(2\pi)$. (c) A parametric plot of $f_{12}(t)$ and $f_{23}(t)$ versus $\delta B_z(t)$ by combining analysis of (a) and (b). Solid curves in (b) and (c) are theoretical splittings from an eigenspectrum calculation, provided only $f_{\rm rf}$, $B_z(t)$, and Ω, i.e. no free parameters. Variation of the synthetic clock transition f_{12} for $0 \le \delta B_z \le B_{\rm rf}/4 = 3.2\,$mG (c, inset).

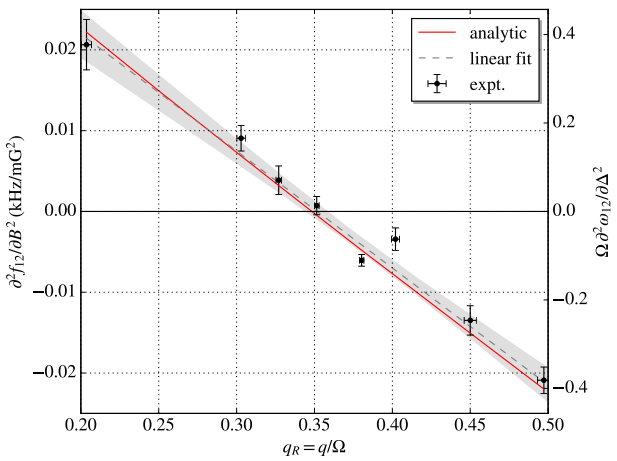

FIG. 4. Curvature of the synthetic clock transition for normalized quadratic shifts $q_R \in [0.2, 0.5]$. The measured curvature (black points) was determined from polynomial fitting to $(\delta B_z, f_{12})$ data shown in Fig. 3(c). Vertical and horizontal error bars correspond to the standard error of the regression and uncertainty in q_R (via $u(q)$ and $u(\Omega)$ at each field B_0), respectively. A linear fit (black, dashed) with 1σ confidence band (gray, shaded) are shown, whose intercept can be used to impute $q_{R,\rm magic}$ (expt.) $= 0.350(6)$. The analytic expression for the curvature (red) is consistent with the data-driven analysis of the curvature, *cf.* $q_{R,\rm magic}$ (theory) $= 0.348$. The left [right] vertical axis shows the curvature $\partial^2 f_{12}/\partial B_z^2$ [$\Omega\,\partial^2\omega_{12}/\partial\Delta^2$] in absolute units of kHz/G^2 [dimensionless units]. The normalized curvature is unity when $q_R = 0$.

and ac magnetometry bandwidths. The normalized variation $\omega_{12}/\Omega = 8.6 \times 10^{-3}$ (expt.) and 5.8×10^{-3} (theory) across a detuning range of ~~$0 \le |\Delta/\Omega| \le 0.5$~~half a Rabi frequency. By comparison, the normalized variation ~~at~~ for conventional decoupling ($q_R = 0$) is $(\sqrt{5}-2)/2 \approx 0.118$; 14 (expt.) and 20 (theory) times higher than the ~~observed predicted~~variation. Alternatively, the normalized variation of the $|m_z = \pm 1\rangle \leftrightarrow |m_z = 0\rangle$ Zeeman transitions ~~at $q = 0$~~ in the low-field limit is 0.5; 58 (expt.) and 86 (theory) times higher than the ~~observed predicted~~variation in the synthetic clock transition frequency.

~~In the adiabatic limit, the dressed state populations remain constant and the above superposition evolves under phase acquisition $e^{-i\omega_i t}$ by each dressed state $|i\rangle$ [29]. We quantify the stasis of the dressed superposition using the generalized adiabatic parameter $\Gamma \equiv |\mathbf{\Omega}(t)/\dot{\theta}(t)|$, where $\mathbf{\Omega} = \mathbf{B}_{\rm eff}/\gamma \equiv \Omega\,\mathbf{e}_x + \Delta\,\mathbf{e}_z$ and $\tan\theta \equiv \Omega/\Delta$. (The adiabatic limit is $\Gamma \gg 1$.) For constant coupling amplitude $\dot{\Omega} = 0$, $\dot{\theta}(t) = -\Omega\dot{\Delta}(t)/|\mathbf{\Omega}|^2$. For the magnetic field sweeps used here, Γ exceeded 200 at all times and was on average $\gtrsim 600$. Nevertheless, the continuous spectra when plotted parametrically (c) exhibit some evidence of non-adiabatic following. Numerical integration of the Schrödinger equation of the known control Hamiltonian confirms that dressed state populations vary slowly (compared to ω_D^{-1}) and deviate by no more than several percent from their initial values near minima of $\Gamma(t)$.~~

~~To test the predictive power of our measurement of dynamical decoupling, we determined the curvature of the synthetic clock transition with respect to magnetic~~ To optimally suppress the sensitivity of the synthetic clock

states to small field variations, ~~inspecting the quadratic coefficient of a polynomial fit to $(\delta B_z, f_{12})$ data. The results of this model independent analysis are shown in~~ we experimentally determined the curvature of ω_{12} for q_R between 0.2 and 0.5~~. The curvature $\partial^2 f_{12}/\partial B_z^2$ is predicted analytically to be near-linear in~~, independent of the predicted spectrum of $\mathcal{H}_{\rm rwa}$. For each q_R~~over this range. Accordingly, we~~, we fit a polynomial to $(\delta B_z, f_{12})$ data to extract $\partial^2 f_{12}/\partial B_z^2$ (Fig. 4). The predictive power of the measured dressed spectrum and this model-independent analysis is affirmed by the agreement with the theoretical curvature. We perform linear regression ~~to~~ of the measured curvature versus q_R to infer ~~$q_{R,\rm magic}$, where the synthetic clock transition has vanishing curvature, and find~~ $q_{R,\rm magic}$ (expt.) $= 0.350(6)$, in agreement with the theoretical value in Eq. (1). The ~~minimum curvature measured occurred~~ lowest curvature we measured was $\left(\partial^2 f_{12}/\partial B_z^2\right)_{\rm min} = 1\,{\rm Hz/mG^2}$ at $q_R = 0.351(2)$~~, with a value of $\left(\partial^2 f_{12}/\partial B_z^2\right)_{\rm min} = 1\,{\rm Hz/mG^2}$.~~. In dimensionless units – with the splitting and detuning normalized to the Rabi frequency – $\left(\Omega\,\partial^2\omega_{12}/\partial\Delta^2\right)_{\rm min} = 0.02$, fifty times lower than the curvature of this transition for ~~the second-order decoupled~~ quadratic decoupling $(q_R = 0)$~~case~~.

~~Despite long coherence times, the low duty cycle $(D < 0.01)$ and low repetition rate $(T_{\rm shot} \gtrsim 10\,{\rm s})$ of cold quantum gas experiments make it challenging to achieve metrological sensitivities per unit bandwidth that are competitive with other platforms. Here $D = 0.005$ and $T_{\rm shot} = 20\,{\rm s}$, yet we make many more spin projection measurements (at a shot-noise limited SNR of 10–100 [25]) than traditional cold atom experiments ($N_m = 1$ to several, e.g. absorption or dispersive imaging).~~ This intra-shot revelation of the time and frequency domain renders the measurement of these spectra orders of magnitude more efficient. For example, the single spectrum shown in Fig. 3 would take $\sim$ (10 shots per δB_z per ~~ω_{ij}) $\times$ (100~~ ω_{ij}) $\times$ (20 distinct δB_z~~values~~) $\times$(3 transitions ~~ω_{ij}) $= 3000$~~ ω_{ij}) $= 600$ shots, or ~~$\sim 6 \times 10^4\,{\rm s} = 1000$~~ $\sim 1.2 \times 10^4\,{\rm s} = 200$ minutes of data acquisition. We acquire this spectrum in a single shot, i.e. 20 s. The data used to generate Fig. 4 was acquired in only 5 minutes.

In summary, we have demonstrated real-time measurement of continuous dynamical decoupling in a spin-1 quantum gas, and expeditious optimization of this decoupling by varying the the relative asymmetry of the Zeeman state splittings. Continuous weak measurement via the Faraday effect yields information about the rf-dressed superposition, the dressed-state couplings and energies, simultaneously. In this measurement regime, we do not resolve the quantum noise of the decoupled collective spin. With a modification of the probe (atom-shot noise dominated) we could measure and affect the quantum noise dynamically, and probing the dressed state coherences in this regime may expose non-Gaussian quantum noise geometries in a manner analogous to Ref. [30]. Our time-frequency reduction of the weak measurement record make plain the cyclic coupling of all three dressed states, which could be applied to emulating quantum spin ladders with frustrated interactions. By making the coupling spatially dependent, the optimal decoupling of the synthetic clock states demonstrated can be applied to critical phenomena in spin-orbit coupled spin-1 Bose gases, as $q = q_{R,\rm magic}\Omega$ traverses the polar-striped and plane-wave phases in the vicinity of a tricritical point of the (Ω, q) phase diagram [31]. Indeed the Faraday probe beam – used to detect magnetization – could constitute one of the Raman beams used to generate the spin-orbit coupling.

[1] M. J. Biercuk, H. Uys, A. P. VanDevender, N. Shiga, W. M. Itano, and J. J. Bollinger, Nature **458**, 996 (2009).

[2] G. d. Lange, Z. H. Wang, D. Ristè, V. V. Dobrovitski, and R. Hanson, Science **330**, 60 (2010).

[3] H. Bluhm, S. Foletti, I. Neder, M. Rudner, D. Mahalu, V. Umansky, and A. Yacoby, Nature Physics **7**, 109 (2011).

[4] F. F. Fanchini, J. E. M. Hornos, and R. d. J. Napolitano, Physical Review A **75**, 022329 (2007).

[5] M. Hirose, C. D. Aiello, and P. Cappellaro, Physical Review A **86**, 062320 (2012).

[6] M. Loretz, T. Rosskopf, and C. L. Degen, Physical Review Letters **110**, 017602 (2013).

[7] J.-M. Cai, B. Naydenov, R. Pfeiffer, L. P. McGuinness, K. D. Jahnke, F. Jelezko, M. B. Plenio, and A. Retzker, New Journal of Physics **14**, 113023 (2012); J. Cai, F. Jelezko, N. Katz, A. Retzker, and M. B. Plenio, New Journal of Physics **14**, 093030 (2012).

[8] D. A. Golter, T. K. Baldwin, and H. Wang, Physical Review Letters **113**, 237601 (2014).

[9] N. Aharon, M. Drewsen, and A. Retzker, Physical Review Letters **111**, 230507 (2013).

[10] P. Facchi and S. Pascazio, Physical Review Letters **89**, 080401 (2002); P. Facchi, D. A. Lidar, and S. Pascazio, Physical Review A **69**, 032314 (2004).

[11] R. Vijay, C. Macklin, D. H. Slichter, S. J. Weber, K. W. Murch, R. Naik, A. N. Korotkov, and I. Siddiqi, Nature **490**, 77 (2012).

[12] A. Valdés-Curiel, D. Trypogeorgos, E. E. Marshall, and I. B. Spielman, New Journal of Physics **19**, 033025 (2017).

[13] C. F. Ockeloen, R. Schmied, M. F. Riedel, and P. Treutlein, Physical Review Letters **111**, 143001 (2013); A. Horsley and P. Treutlein, Applied Physics Letters **108**, 211102 (2016).

[14] D. M. Stamper-Kurn and M. Ueda, Reviews of Modern Physics **85**, 1191 (2013).

[15] H.-J. Mikeska and A. K. Kolezhuk, in *Quantum Magnetism*, Lecture Notes in Physics No. 645, edited by U. Schollwöck, J. Richter, D. J. J. Farnell, and R. F. Bishop (Springer Berlin Heidelberg, 2004) pp. 1–83.

[16] E. Majorana, Il Nuovo Cimento (1924-1942) **9**, 43 (1932).

[17] J. M. Boss, K. S. Cujia, J. Zopes, and C. L. Degen, Science **356**, 837 (2017); S. Schmitt, T. Gefen, F. M. Stürner, T. Unden, G. Wolff, C. Müller, J. Scheuer, B. Naydenov, M. Markham, S. Pezzagna, J. Meijer, I. Schwarz, M. Plenio, A. Retzker, L. P. McGuinness, and F. Jelezko, Science **356**, 832 (2017).

[18] N. Ramsey, *Molecular beams* (Clarendon Press, 1956).

[19] F. Gerbier, A. Widera, S. Fölling, O. Mandel, and I. Bloch, Physical Review A **73**, 041602 (2006).

[20] G. A. Smith, S. Chaudhury, A. Silberfarb, I. H. Deutsch, and P. S. Jessen, Physical Review Letters **93**, 163602 (2004).

[21] P. Rabl, P. Cappellaro, M. V. G. Dutt, L. Jiang, J. R. Maze, and M. D. Lukin, Physical Review B **79**, 041302 (2009); X. Xu, Z. Wang, C. Duan, P. Huang, P. Wang, Y. Wang, N. Xu, X. Kong, F. Shi, X. Rong, and J. Du, Physical Review Letters **109**, 070502 (2012).

[22] The curvature of the dressed-state energies is evaluated using perturbation theory. In particular, the dimensionless curvature of ω_{12} is $\partial^2(\omega_{12}/\Omega)/\partial(\Delta/\Omega)^2 = \Omega\,\partial^2\omega_{12}/\partial\Delta^2 = -(3q_R\sqrt{4+q_R^2} - q_R^2 - 2)/(2\sqrt{4+q_R^2})$. For $q_R = 0$, we recover the spin-1/2 result, $\Omega\,\partial^2\omega_{12}/\partial\Delta^2 = 1$.

[23] We take $\Delta = -\gamma\,\delta B_z$ for $|\Delta| \leq 2\Omega$ ($|\delta B_z| \leq B_{\rm rf}/2$) and $|\partial q/\partial\Delta| \approx |\gamma^{-1}\partial q/\partial B_z| = |2B_z q_Z/\gamma| \ll 1$, valid to 10^{-3} for the field strengths $B_z \lesssim 5\,\mathrm{G}$ used here, resulting in vanishing third-order derivatives of ω_i with respect to detuning. In general, the variation of q with Δ (or δB_z) can be accounted for using the Breit-Rabi equation, leading to a residual linear and cubic variation of ω_{12} with δB_z, and a small correction to $q_{R,\rm magic}$ in Eq. (1).

[24] A. A. Wood, L. M. Bennie, A. Duong, M. Jasperse, L. D. Turner, and R. P. Anderson, Physical Review A **92**, 053604 (2015).

[25] M. Jasperse, M. J. Kewming, S. N. Fischer, P. Pakkiam, R. P. Anderson, and L. D. Turner, arXiv:1705.10965 (2017).

[26] Y. Liu, S. Jung, S. E. Maxwell, L. D. Turner, E. Tiesinga, and P. D. Lett, Physical Review Letters **102**, 125301 (2009); G. A. Smith, A. Silberfarb, I. H. Deutsch, and P. S. Jessen, Physical Review Letters **97**, 180403 (2006).

[27] T. Dimitris, A. Valdés-Curiel, N. Lundblad, and I. B. Spielman, arXiv:1706.xxxxx (2017).

[28] The experiment is synchronized to the mains power line; the harmonic composition ~~of which~~ varies little between ~~contiguous~~ successive shots (20 s apart), and thus the ~~measured~~ calibration $\delta B_z(t)$ and $q(t)$ ~~from the calibration shot serve as a~~ are good ~~proxy~~ proxies for the values experienced by the atoms in the subsequent decoupled shot.

[29] A. Messiah, *Quantum mechanics*, Vol. 2 (North-Holland, 1962).

[30] G. Colangelo, F. M. Ciurana, L. C. Bianchet, R. J. Sewell, and M. W. Mitchell, Nature **543**, 525 (2017).

[31] G. I. Martone, Physical Review Letters **117** (2016), 10.1103/PhysRevLett.117.125301.